Hindawi
International Journal of Antennas and Propagation
Volume 2019, Article ID 6181435, 9 pages
https://doi.org/10.1155/2019/6181435

Research Article

Characterization of Slow and Fast Fading in Off-Body Communication at 2.45 GHz with Space Diversity Scheme in an Indoor Environment

Szymon Wiszniewski and Slawomir J. Ambroziak

Faculty of Electronics, Telecommunications and Informatics, Gdansk University of Technology, Gdansk, Poland

Correspondence should be addressed to Szymon Wiszniewski; szywiszn@pg.edu.pl

Received 10 December 2018; Accepted 23 December 2018; Published 21 February 2019

Academic Editor: Luciano Tarricone

The characterization of slow and fast fading in wireless body area networks with space diversity scheme has been presented. The analysis, based on the measurements at 2.45 GHz in an indoor environment, has shown that for all investigated configurations of receiving wearable antennas, the correlation coefficient values of the received signals' parameters are below the assumed value of 0.5, being close to zero for the vast majority of cases. It has been shown that the slow fading component may be modelled by a lognormal distribution with zero average and the standard deviation from the range of [1.43, 1.98] dB. The fast fading component is the best modelled by a Rice distribution with the noncentrality parameter and the scale parameter being in the range [0.8125, 0.9624] and [0.5269, 0.6954], respectively.

1. Introduction

Nowadays, when the wireless body area networks (WBANs) become more and more popular, and the amount of the wearable sensors used by people are increasing, there is a need to model the radio channel around the human body with higher accuracy. The human body itself and its motion should be considered as significant elements that influence the total system loss in WBANs [1]. Since there are applications of such networks (e.g., the healthcare [2] or military), in which the proper radio coverage and the errorless communication are of the high importance, the accurate modeling of radio channel becomes crucial.

The various diversity schemes, that can be used in off-body communications in WBANs, can significantly increase the quality of the received signals. This technique allows receiving uncorrelated replicas of the same radio signal and, in addition to one of the possible combining methods, can significantly increase the signal-to-noise ratio. It is very useful especially when the multipath propagation occurs. Depending on the signal decorrelation method, one can distinguish polarization diversity or space diversity. In this article, the concept of the space diversity scheme in WBANs has been presented. Additionally, the characterization of the slow and fast fading for different placements of the received antennas has been performed.

There are some research work on the space diversity concept, but they are focused on in-body to on-body [3] or on-body communication [4, 5]. The off-body communication is taken into account in [6]; however, there is a limited number of considered receiving antennas' positions, i.e., two receiving antennas have been placed on the chest. Moreover, the current standard for WBANs, [7] does not raise the issue of channel models with diversity schemes. The novelty of the article is the investigation of the influence of different mutual positions of the receiving antennas on the correlation of slow and fast fading of received signal.

The rest of the article is structured as follows. In the next section, the measurement stand, scenarios, and investigated environment have been briefly described. The third section consists the description of the measurement data processing. The analysis of the correlation coefficient between the

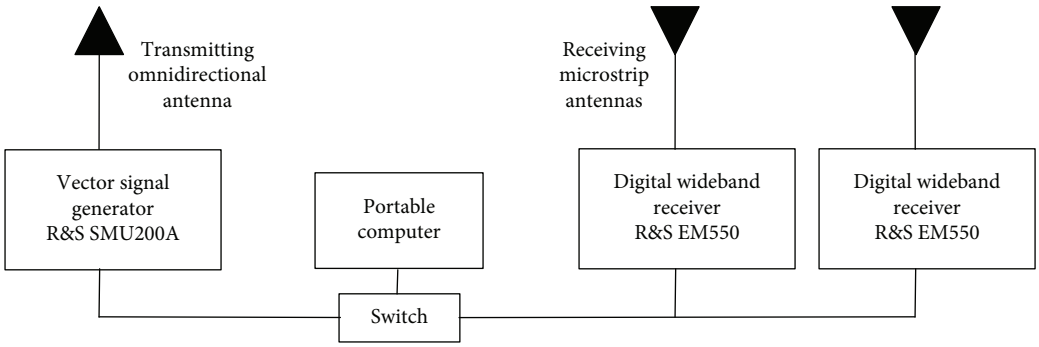

Figure 1: Measurement stand for space diversity investigations.

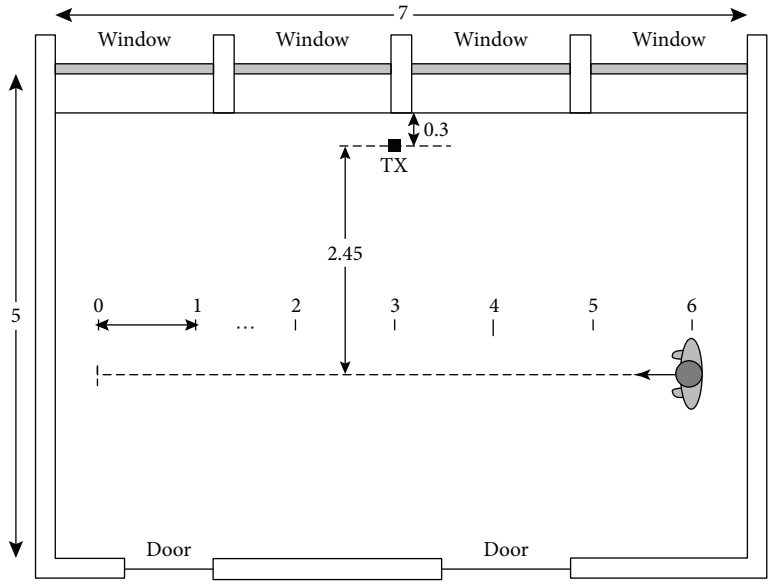

Figure 2: Layout of the investigated indoor environment (dimensions are in meters).

received signal parameters obtained by different antennas is presented in the following section. The last part of the paper consists of the summary and concluding remarks.

2. Description of the Measurements

The measurement stand used for the space diversity investigations has been presented in Figure 1. The detailed description of the equipment may be found in [8]. In the article, only the most important parameters have been presented.

The transmitting (TX) section consists of the vector signal generator (Rohde & Schwartz SMU200A) and the omnidirectional, linear polarized antenna (Cobham OA2-0.3-10.0V/1505), with a 2 dBi gain and half-power beam width of 360° and 65° in the H- and E-planes, respectively. It has been designed for operation in the frequency range of 0.3-10.0 GHz. The generator provides the RF signal with BPSK modulation at 2.45 GHz frequency, modulated by the pseudorandom sequence with the 23 bit of length and 3 kbit/s rate.

The receiving (RX) section consists of two wideband receivers (Rohde & Schwartz EM550), connected to the wearable patch antennas, operating at 2.45 GHz frequency. These antennas have linear polarization, 3 dBi gain, and half-power beam width of 115° and 40° in the H- and E-planes, respectively.

Table 1: Positions of RX antennas for different space diversity configurations.

Configuration	Position of RX antenna no. 1	Position of RX antenna no. 2
C1	TO_F	TO_B
C2	TO_F	AB_L
C3	TO_F	AB_R
C4	TO_F	HE_L
C5	TO_F	HE_R
C6	TO_B	AB_L
C7	TO_B	AB_R
C8	TO_B	HE_L
C9	TO_B	HE_R

(a) (b)

Figure 3: Exemplary placements of receiving antennas for configurations C2 (a) and C4 (b).

Table 2: Probability distributions functions selected for L_{sf} and L_{ff} analysis.

Name of PDF	PDF parameters	
Rice	Noncentrality parameter: s_{Rice}	Scale parameter: σ_{Rice}
Nakagami-m	Shape parameter: m	Scale parameter: Ω
Weibull	Shape parameter: b	Scale parameter: a
Rayleigh	Scale parameter: σ_{Ray}	—
Lognormal	Mean [dB]: μ_L	Standard deviation [dB]: σ_L

All RF connections have been realized by the 10 m long high-frequency cable SUCOFLEX 126E with the attenuation of 4 dB at the investigated frequency. Obviously, this value has been taken into account during the calibration process.

The measurements were performed in a typical indoor office environment, with the following dimensions: $7 \times 5 \times 3\,m^3$. Two receiving antennas were placed on one user, with a height of 1.65 m and a weight of 64 kg. In Figure 2, the layout of the investigated indoor environment has been presented.

During measurements, the dynamic scenario has been investigated—the user was walking ten times along the axis of the room in the direction indicated in Figure 2. The TX antenna was mounted in the middle of the room, at 2.6 m close to the wall. The six most popular RX antenna placements have been considered: torso front (TO_F), torso back (TO_B), bottom part of the left arm (AB_L), bottom part of the right arm (AB_R), left side of the head (HE_L), and right side of the head (HE_R). Based on the above antenna locations, nine space diversity configurations (C1–C9) have been defined in Table 1.

In Figure 3, one can see the RX antennas mounted on the user body for configurations C2 and C4.

3. Measurement Data Processing

This section describes how the slow and fast fading components have been extracted from the instantaneous system loss values, L_{SL}. Firstly, the mean system loss, $\overline{L_{SL}(d)}$, has been obtained by fitting a logarithmic function of distance to the composite component, $\overline{L_{CSL}}$, which is a space-averaged values of total system loss, where the averaging window width is taken as a 5-wavelength interval. It should be noted that this fitting has been performed separately for the cases of user approaching to and departing from the transmitting antenna, when the distance was increasing and decreasing, respectively. Next, the slow fading component, L_{sf}, has been extracted by subtracting the mean system loss from the composite component, what may be expressed as follows:

$$L_{sf[dB]} = \overline{L_{SL}(d)_{[dB]}} - \overline{L_{CSL[dB]}}. \quad (1)$$

Table 3

(a) Results of the fast fading distribution fitting for configurations C1–C4

Configuration	RX ant.	Distribution	Parameters				χ^2	χ^2_{crit}	*AIC*	Correlation
C1	TO_F	**Rice**	$\mathbf{s_{Rice}}$	**0.9602**	$\boldsymbol{\sigma_{Rice}}$	**0.5269**	**21.19**	**27.59**	**19389**	**0.98**
		Nakagami	m	1.1750	Ω	1.4772	15.81	27.59	20474	0.90
		Weibull	a	1.2479	b	2.4021	18.39	27.59	20056	0.95
		Rayleigh	σ_{Ray}	0.8594	—	—	13.35	28.87	20689	0.83
	TO_B	**Rice**	$\mathbf{s_{Rice}}$	**0.8943**	$\boldsymbol{\sigma_{Rice}}$	**0.6212**	**27.69**	**27.59**	**22092**	**0.98**
		Nakagami	m	1.0356	Ω	1.5714	22.17	27.59	22551	0.93
		Weibull	a	1.2704	b	2.1638	24.73	27.59	22438	0.96
		Rayleigh	σ_{Ray}	0.8864	—	—	21.26	28.87	22560	0.92
C2	TO_F	**Rice**	$\mathbf{s_{Rice}}$	**0.9129**	$\boldsymbol{\sigma_{Rice}}$	**0.5661**	**19.12**	**27.59**	**20517**	**0.98**
		Nakagami	m	1.1325	Ω	1.4743	15.25	27.59	21207	0.90
		Weibull	a	1.2415	b	2.3043	17.36	27.59	20945	0.94
		Rayleigh	σ_{Ray}	0.8586	—	—	13.12	28.87	21339	0.86
	AB_L	**Rice**	$\mathbf{s_{Rice}}$	**0.8918**	$\boldsymbol{\sigma_{Rice}}$	**0.6090**	**25.74**	**27.59**	**21938**	**0.99**
		Nakagami	m	1.0614	Ω	1.5371	20.98	27.59	22432	0.93
		Weibull	a	1.2593	b	2.1956	23.32	27.59	22287	0.96
		Rayleigh	σ_{Ray}	0.8767	—	—	19.61	28.87	22462	0.91
C3	TO_F	**Rice**	$\mathbf{s_{Rice}}$	**0.9475**	$\boldsymbol{\sigma_{Rice}}$	**0.5493**	**22.04**	**27.59**	**22173**	**0.97**
		Nakagami	m	1.1249	Ω	1.5012	16.53	27.59	23224	0.87
		Weibull	a	1.2537	b	2.3339	19.20	27.59	22856	0.93
		Rayleigh	σ_{Ray}	0.8664	—	—	14.54	28.87	23351	0.81
	AB_R	**Rice**	$\mathbf{s_{Rice}}$	**0.8651**	$\boldsymbol{\sigma_{Rice}}$	**0.6488**	**27.45**	**27.59**	**24718**	**0.98**
		Nakagami	m	1.0225	Ω	1.5903	22.44	27.59	25098	0.94
		Weibull	a	1.2752	b	2.1318	25.14	27.59	25013	0.96
		Rayleigh	σ_{Ray}	0.8917	—	—	21.71	28.87	25101	0.94
C4	TO_F	**Rice**	$\mathbf{s_{Rice}}$	**0.9624**	$\boldsymbol{\sigma_{Rice}}$	**0.5346**	**20.00**	**27.59**	**21404**	**0.95**
		Nakagami	m	1.1202	Ω	1.4977	14.39	27.59	22688	0.81
		Weibull	a	1.2530	b	2.3608	17.00	27.59	22257	0.89
		Rayleigh	σ_{Ray}	0.8654	—	—	12.80	28.87	22804	0.76
	HE_L	**Rice**	$\mathbf{s_{Rice}}$	**0.8319**	$\boldsymbol{\sigma_{Rice}}$	**0.6909**	**27.00**	**27.59**	**25501**	**0.98**
		Nakagami	m	0.9525	Ω	1.6467	21.39	27.59	25705	0.94
		Weibull	a	1.2872	b	2.0339	23.73	27.59	25722	0.96
		Rayleigh	σ_{Ray}	0.9074	—	—	22.88	28.87	25726	0.95

(b) Results of the fast fading distribution fitting for configurations C5–C9

Configuration	RX ant.	Distribution	Parameters				χ^2	χ^2_{crit}	*AIC*	Correlation
C5	TO_F	**Rice**	$\mathbf{s_{Rice}}$	**0.9203**	$\boldsymbol{\sigma_{Rice}}$	**0.5614**	**22.99**	**27.59**	**21081**	**0.96**
		Nakagami	m	1.1532	Ω	1.4772	18.61	27.59	21843	0.88
		Weibull	a	1.2451	b	2.3400	21.23	27.59	21529	0.92
		Rayleigh	σ_{Ray}	0.8594	—	—	15.84	28.87	22022	0.82

Table 3: Continued.

Configuration	RX ant.	Distribution	Parameters				χ^2	χ^2_{crit}	*AIC*	Correlation
		Rice	s_{Rice}	**0.9106**	σ_{Rice}	**0.5737**	**24.84**	**27.59**	**21534**	**0.97**
		Nakagami	m	1.1224	Ω	1.4874	20.08	27.59	22225	0.90
	HE_R	Weibull	a	1.2461	b	2.2924	22.80	27.59	21966	0.94
		Rayleigh	σ_{Ray}	0.8624	—	—	17.50	28.87	22344	0.85
		Rice	s_{Rice}	**0.9200**	σ_{Rice}	**0.5503**	**19.75**	**27.59**	**21571**	**0.97**
		Nakagami	m	1.1620	Ω	1.4521	15.84	27.59	22399	0.89
	TO_B	Weibull	a	1.2351	b	2.3490	17.97	27.59	22062	0.94
		Rayleigh	σ_{Ray}	0.8521	—	—	13.51	28.87	22606	0.83
C6		**Rice**	s_{Rice}	**0.8445**	σ_{Rice}	**0.6828**	**24.46**	**27.59**	**26078**	**0.98**
		Nakagami	m	0.9567	Ω	1.6456	19.31	27.59	26314	0.94
	AB_L	Weibull	a	1.2878	b	2.0434	21.40	27.59	26324	0.96
		Rayleigh	σ_{Ray}	0.9071	—	—	20.46	28.87	26332	0.95
		Rice	s_{Rice}	**0.9240**	σ_{Rice}	**0.5803**	**25.60**	**27.59**	**22718**	**0.98**
		Nakagami	m	1.0866	Ω	1.5272	19.82	27.59	23490	0.90
	TO_B	Weibull	a	1.2598	b	2.2595	22.76	27.59	23243	0.94
		Rayleigh	σ_{Ray}	0.8739	—	—	17.92	28.87	23552	0.86
C7		**Rice**	s_{Rice}	**0.8772**	σ_{Rice}	**0.6334**	**29.30**	**27.59**	**23859**	**0.99**
		Nakagami	m	1.0495	Ω	1.5719	24.49	27.59	24278	0.94
	AB_R	Weibull	a	1.2712	b	2.1669	27.04	27.59	24161	0.97
		Rayleigh	σ_{Ray}	0.8865	—	—	23.06	28.87	24298	0.93
		Rice	s_{Rice}	**0.9285**	σ_{Rice}	**0.5585**	**22.17**	**27.59**	**21709**	**0.98**
		Nakagami	m	1.1337	Ω	1.4860	17.37	27.59	22553	0.89
	TO_B	Weibull	a	1.2471	b	2.3203	19.86	27.59	22240	0.94
		Rayleigh	σ_{Ray}	0.8620	—	—	15.10	28.87	22695	0.84
C8		**Rice**	s_{Rice}	**0.8125**	σ_{Rice}	**0.6954**	**29.38**	**27.59**	**25188**	**0.99**
		Nakagami	m	0.9802	Ω	1.6274	24.55	27.59	25382	0.97
	HE_L	Weibull	a	1.2821	b	2.0552	26.84	27.59	25370	0.98
		Rayleigh	σ_{Ray}	0.9020	—	—	25.26	28.87	25384	0.97
		Rice	s_{Rice}	**0.9221**	σ_{Rice}	**0.5469**	**22.68**	**27.59**	**20419**	**0.98**
		Nakagami	m	1.1964	Ω	1.4485	18.64	27.59	21173	0.91
	TO_B	Weibull	a	1.2362	b	2.3858	21.15	27.59	20828	0.95
		Rayleigh	σ_{Ray}	0.8510	—	—	15.25	28.87	21453	0.84
C9		**Rice**	s_{Rice}	**0.9027**	σ_{Rice}	**0.5988**	**27.07**	**27.59**	**22514**	**0.97**
		Nakagami	m	1.0737	Ω	1.5320	21.66	27.59	23121	0.89
	HE_R	Weibull	a	1.2595	b	2.2254	24.58	27.59	22932	0.93
		Rayleigh	σ_{Ray}	0.8752	—	—	19.80	28.87	23165	0.86

Finally, the fast fading component, also known as a multipath fading component, L_{ff}, has been obtained by subtracting the composite component from the instantaneous values of the measured system loss, i.e.,

$$L_{ff[dB]} = L_{SL[dB]} - \overline{L_{CSL[dB]}}. \quad (2)$$

For statistical analysis of the slow and fast fading, the most commonly used probability distribution functions (PDFs) were taken into consideration [9–13]. Table 2 presents the selected PDFs and their parameters [14].

The Rice, Nakagami-*m*, Weibull, and Rayleigh distributions have been used to characterize the multipath fading, while the lognormal distribution has been used with

respect to the slow fading. The fitting of the empirical distributions of slow and fast fading has been evaluated by the use of the χ^2 and correlation tests. Additionally, the Akaike Information Criterion (AIC) has been used in order to select the best-fitted distribution among those that have passed the abovementioned tests.

4. Results Analysis

4.1. Fast Fading Characteristics. The results of PDFs fitting for the fast fading component are presented in Table 3(a) (for configurations C1–C4) and Table 3(b) (for configurations C5–C9). Both tables include the distribution parameters and the results of evaluation tests. The χ^2, χ^2_{crit}, and *AIC* stand for the χ^2 test statistics, the critical value of this statistics for the significance level of 5%, and the AIC statistic, respectively. It should be reminded that the χ^2 test is passed when the value of χ^2 statistics is below the critical value, and the lowest AIC value indicates the best-fitted PDF [15]. The name of the distributions with the best-fitting results for each configuration has been bolded in the Table 3.

For all analyzed cases, the χ^2 test has been passed, except for TO_B in C1 configuration, where the statistics value is comparable with the critical one, but slightly higher. Considering the AIC values, as well as the correlation test for all configurations and RX antennas' positions, the best-fitted distribution for fast fading component is Rice. It was expected since for the analyzed scenarios and environment there is a high probability of the existence of strong dominant component in the received signal. The noncentrality parameter, s_{Rice}, whose squared value corresponds to the power of dominant component of received signal, is in the range from 0.8125 (for C8-HE_L) up to 0.9624 (for C4-TO_F configuration). On the other hand, the scale parameter, σ_{Rice}, whose doubled-squared value corresponds to the power of scattered components, is between 0.5269 (for C1-TO_F) and 0.6954 (for C8-HE_L configuration). The abovementioned values show that, for each case, the power of dominant component is higher than the power of the scattered ones.

Figure 4 shows the exemplary graph of the selected PDFs (Rice, Nakagami, Weibull, and Rayleigh) fitted to the empirical distribution of the fast fading magnitude in linear scale, α. As one can see, the shape of the Rice distribution is the closest to the empirical one, what is expected after consideration of the numerical data from Tables 3(a) and 3(b).

4.2. Slow Fading Characteristics. Analogous results of the lognormal distribution fitting for the slow fading component have been gathered in Table 4. For all cases, the χ^2_{crit} value is the same and equals 27.59 for a significance level of 5%.

Since the values of χ^2 statistics are below the critical value for all the cases, and the correlation is over 95% for the vast majority of them, one can say that the lognormal distribution fits well to the empirical one. Moreover, the average of the slow fading component (μ_L) is close to zero in the log domain for all configurations. It confirms that the slow fading component have been obtained properly in the data processing

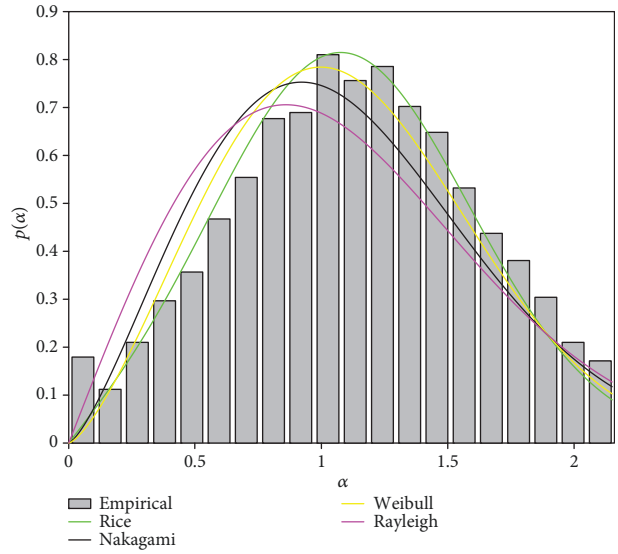

Figure 4: Exemplary fast fading distributions for C1 configuration and RX antenna placed on TO_F.

phase. On the other hand, the standard deviation of the slow fading component (σ_L) is below 2 dB, being in the range of [1.43, 1.98] dB, which is a relatively low value.

In Figure 5, the exemplary graph of the lognormal PDF fitting to the empirical distribution of the slow fading magnitude (α), obtained from the measurements for the antenna placed on the torso in C1 configuration, has been presented. One can observe the good fitting of both distributions.

4.3. Spatial Decorrelation of Received Signal. In order to realize any of the diversity schemes (spatial, polarization, etc.), one has to ensure the proper decorrelation level of two or more received replicas of radio signal and use one of the well-known diversity combining techniques (e.g., maximal-ratio combining or equal-gain combining). Focusing on the decorrelation issue, it may be assumed that it is sufficient to have the correlation coefficient lower than 0.5, in order to obtain a satisfactory value of the diversity gain. One of the commonly used methods for decorrelation of the received signal's replicas, propagating through different radio paths, is the spatial separation of two (or more) receiving antennas, as it has been done in the presented research.

Table 5 summarizes the correlation coefficient between system loss values (ρ_l), slow fading component (ρ_{sf}), and fast fading component (ρ_{ff}), calculated based on the signals received by two wearable antennas. One can see that for almost all analyzed cases the correlation coefficient values are close to zero, which means that the signals received by two antennas are practically uncorrelated. The outstanding values have been obtained for C1 ($\rho_{sf} = 0.33$), C9 ($\rho_l = -0.11$, $\rho_{sf} = 0.29$, and $\rho_{ff} = -0.14$), and C7 ($\rho_l = -0.15$ and $\rho_{sf} = -0.18$), but even these values are below the assumed threshold of 0.5. Presented results justify the need for the spatial diversity scheme application in WBANs.

The exemplary graphs of the slow and fast fading components in a single scenario realization have been presented in

Table 4: Results of the lognormal distribution fitting for the slow fading component and for all configurations.

Configuration	RX ant.	Parameters				χ^2	Correlation
C1	TO_F	μ_L [dB]	-0.20	σ_L [dB]	1.54	2.67	0.97
	TO_B	μ_L [dB]	-0.19	σ_L [dB]	1.76	5.25	0.97
C2	TO_F	μ_L [dB]	-0.12	σ_L [dB]	1.56	4.92	0.98
	AB_L	μ_L [dB]	-0.16	σ_L [dB]	1.46	1.59	0.98
C3	TO_F	μ_L [dB]	-0.16	σ_L [dB]	1.68	3.88	0.96
	AB_R	μ_L [dB]	-0.21	σ_L [dB]	1.34	1.17	0.98
C4	TO_F	μ_L [dB]	-0.16	σ_L [dB]	1.71	3.78	0.98
	HE_L	μ_L [dB]	-0.23	σ_L [dB]	1.91	4.68	0.95
C5	TO_F	μ_L [dB]	-0.17	σ_L [dB]	1.67	4.02	0.94
	HE_R	μ_L [dB]	-0.11	σ_L [dB]	1.87	11.49	0.70
C6	TO_B	μ_L [dB]	-0.18	σ_L [dB]	1.98	6.78	0.97
	AB_L	μ_L [dB]	-0.17	σ_L [dB]	1.42	2.91	0.95
C7	TO_B	μ_L [dB]	-0.20	σ_L [dB]	1.90	4.09	0.97
	AB_R	μ_L [dB]	-0.22	σ_L [dB]	1.58	3.75	0.98
C8	TO_B	μ_L [dB]	-0.17	σ_L [dB]	1.84	4.91	0.97
	HE_L	μ_L [dB]	-0.20	σ_L [dB]	1.81	4.82	0.96
C9	TO_B	μ_L [dB]	-0.20	σ_L [dB]	1.79	4.10	0.98
	HE_R	μ_L [dB]	-0.13	σ_L [dB]	1.56	4.16	0.97

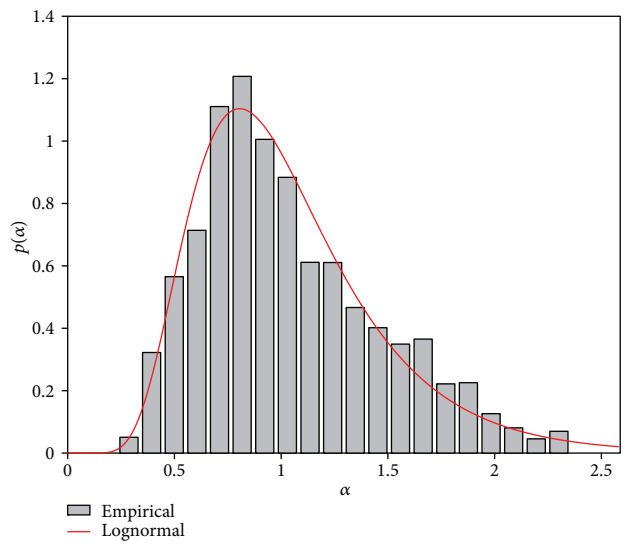

Figure 5: Exemplary slow fading distribution for C9 configuration and antenna placed on TO_B.

Table 5: Correlation coefficient between system loss values (ρ_l), slow fading component (ρ_{sf}), and fast fading component (ρ_{ff}), calculated based on the signals received by two wearable antennas.

Configuration	RX ant.	ρ_l	ρ_{sf}	ρ_{ff}
C1	TO_F-TO_B	-0.07	0.33	-0.01
C2	TO_F-AB_L	0.02	0.03	-0.04
C3	TO_F-AB_R	0.02	0.04	0.00
C4	TO_F-HE_L	0.01	0.06	-0.02
C5	TO_F-HE_R	-0.08	0.08	-0.06
C6	TO_B-AB_L	-0.07	0.03	-0.01
C7	TO_B-AB_R	-0.15	-0.18	-0.04
C8	TO_B-HE_L	-0.10	-0.08	-0.04
C9	TO_B-HE_R	-0.11	0.29	-0.14

Figures 6 and 7, respectively. It may be noticed that in both cases, the magnitudes of fading at the same time are different for particular RX antennas. It confirms graphically the results presented in Table 5.

5. Conclusions

Even though the wireless body area networks are gaining popularity, there are still not many investigations about the space diversity scheme. In situations when the number of wearable devices is getting higher, it is reasonable to consider the use of such a technique to achieve better quality of received signal.

In the article, the characterization of slow and fast fading in WBAN networks with space diversity scheme has been presented. The analysis, based on the measurements at 2.45 GHz in an indoor environment, has also shown that for all investigated configurations, the correlation coefficient values of the received signals' parameters are below the assumed value of 0.5, being close to zero for the vast majority of cases.

It has been shown that the slow fading component may be modelled by a lognormal distribution with zero average and the standard deviation from the range of [1.43,

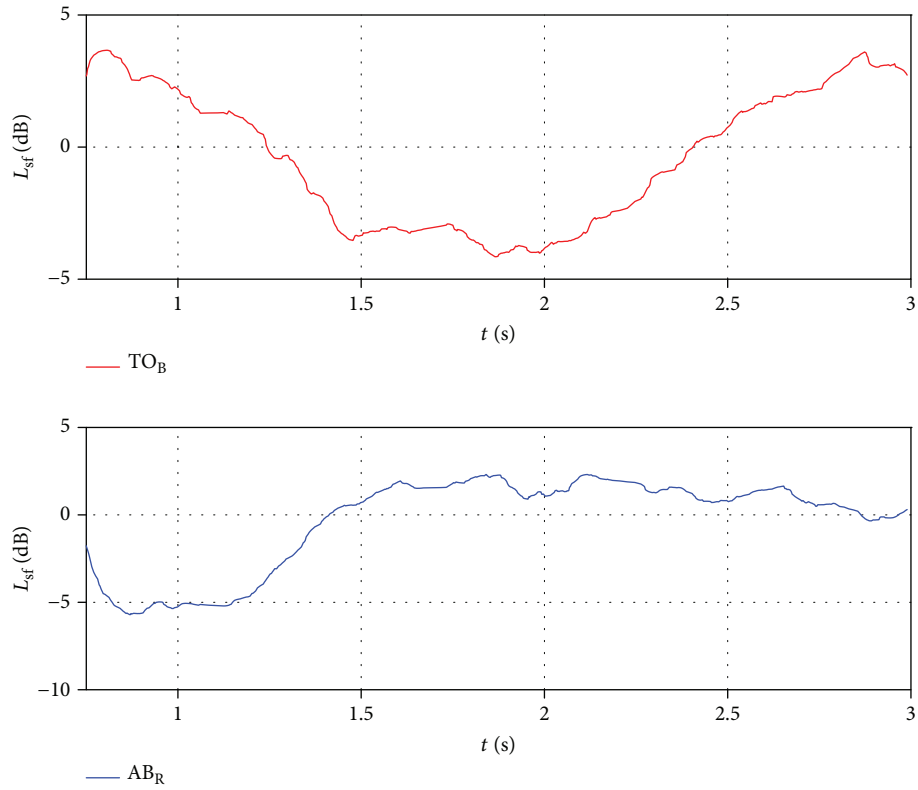

Figure 6: Exemplary graph of the slow fading component in a single realization of scenario for C7.

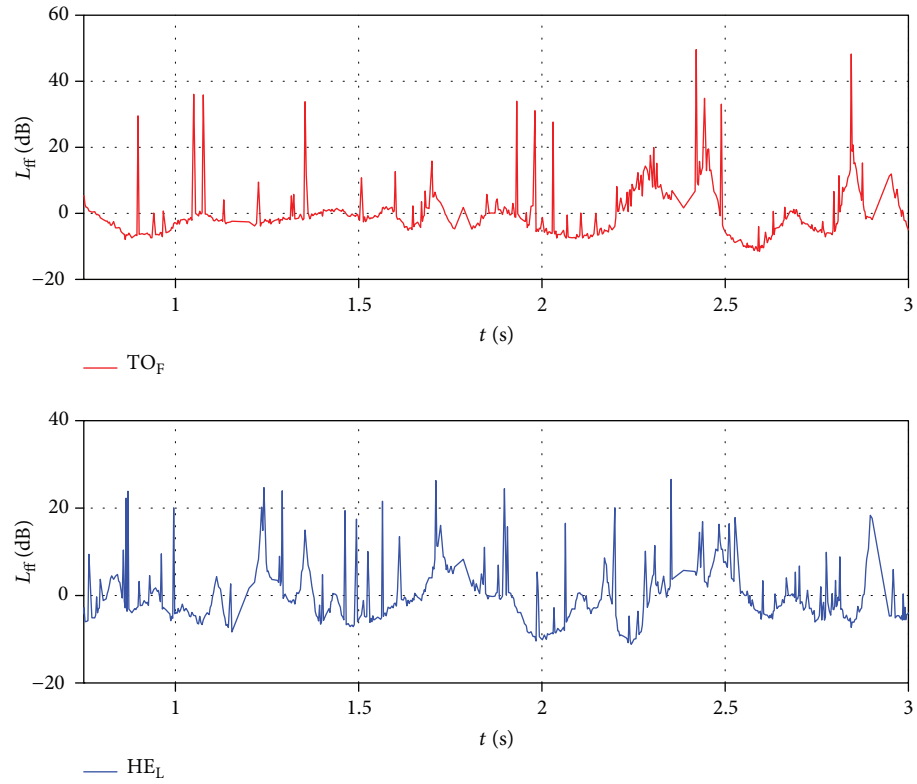

Figure 7: Exemplary graph of the fast fading component in a single realization of scenario for C4.

1.98] dB. The fast fading component is best modelled by a Rice distribution with the noncentrality parameter and the scale parameter being in the range [0.8125, 0.9624] and [0.5269, 0.6954], respectively.

Presented results justify the need for further research in the field of channel modelling in the space diversity scheme and its application in WBANs.

Data Availability

The measurement result data used to support the findings of this study are included within the article.

Conflicts of Interest

The authors declare that there is no conflict of interest regarding the publication of this paper.

References

[1] J. Wang and O. Wang, *Body Area Communications: Channel Modelling, Communications Systems, and EMC*, Wiley, 2013.

[2] M. R. Yuce and J. Y. Khan, *Wireless Body Area Networks: Technology, Implementation, and Applications*, Pan Stanford Publishing, 2012.

[3] J. Shi, D. Anzai, and J. Wang, "Diversity performance of UWB low band communication over in-body to on-body propagation channel," in *2012 6th European Conference on Antennas and Propagation (EUCAP)*, pp. 535–539, Prague, Czech Republic, 2012.

[4] A. Michalopoulou, A. A. Alexandridis, K. Peppas et al., "Statistical analysis for on-body spatial diversity communications at 2.45 GHz," *IEEE Transactions on Antennas and Propagation*, vol. 60, no. 8, pp. 4014–4019, 2012.

[5] S. L. Cotton and W. G. Scanlon, "Characterization and modeling of on-body spatial diversity within indoor environments at 868 MHz," *IEEE Transactions on Wireless Communications*, vol. 8, no. 1, pp. 176–185, 2009.

[6] A. J. Ali, S. L. Cotton, and W. G. Scanlon, "Spatial diversity for off-body communications in an indoor populated environment at 5.8 GHz," in *2009 Loughborough Antennas & Propagation Conference*, pp. 641–644, Loughborough, UK, 2009.

[7] A. Astrin, "IEEE standard for local and metropolitan area networks - part 15.6: wireless body area networks," in *IEEE Std 802.15.6-2012*, IEEE, 2012.

[8] S. Wiszniewski and S. J. Ambroziak, "System loss analysis in body area networks with space diversity scheme," in *2018 Baltic URSI Symposium (URSI)*, pp. 51-52, Poznań, Poland, 2018.

[9] A. Goldsmith, *Wireless Communications*, Cambridge University Press, Cambridge, UK, 2005.

[10] D. B. Smith, D. Miniutti, T. A. Lamahewa, and L. W. Hanlen, "Propagation models for body-area networks: a survey and new outlook," *IEEE Antennas and Propagation Magazine*, vol. 55, no. 5, pp. 97–117, 2013.

[11] M. K. Simon and M.-S. Alouini, *Digital Communication over Fading Channels*, John Wiley & Sons, Inc., 2000.

[12] C. Walck, "Hand-book on statistical distributions for experimentalists," Particle Physics Group, Fysikum, Stockholm University, Tech. Rep. SUF-PFY/96-01, 2007.

[13] *Probability Distributions Relevant to Radiowave Propagation Modelling, document Rec. P. 1057-3*, International Telecommunication Union, Radiocommunication Sector, 2013.

[14] S. J. Ambroziak, L. M. Correia, R. J. Katulski et al., "An off-body channel model for body area networks in indoor environments," *IEEE Transactions on Antennas and Propagation*, vol. 64, no. 9, pp. 4022–4035, 2016.

[15] K. Turbic, S. J. Ambroziak, and L. M. Correia, "Characteristics of the polarised off-body channel in indoor environments," *EURASIP Journal on Wireless Communications and Networking*, vol. 2017, no. 1, 2017.